Arab J Sci Eng (2015) 40:1173–1186
DOI 10.1007/s13369-015-1612-2

RESEARCH ARTICLE - MECHANICAL ENGINEERING

Energy and Exergy Analysis of Solar Air Heaters with Varied Geometries

P. Velmurugan · R. Kalaivanan

Received: 17 November 2014 / Accepted: 4 February 2015 / Published online: 13 February 2015

Abstract An indoor standard test procedure is developed to experimentally investigate the steady state energy and exergy performance of single-pass flat plate solar air heater (SPFPSAH), roughened plate dual-pass solar air heater (RPDPSAH), finned plate dual-pass solar air heater (FPDPSAH) and wire mesh dual-pass solar air heater (WMDPSAH) at varied mass flow rates and solar intensities. The analytical solution of the energy balance equations for various elements of the SPFPSAH, RPDPSAH, FPDPSAH and WMDPSAH is determined using a MATLAB 8.1 program and correlated with experimental findings. The analytical and experimental results show that the energy and exergy performance of WMDPSAH is superior to FPDPSAH, RPDPSAH and SPFPSAH. The pressure drop of WMDPSAH is higher than that of FPDPSAH, RPDPSAH and SPFPSAH. From the economic analysis, WMDPSAH is found economically viable within the opted conditions compared with FPDPSAH and RPDPSAH. The analytical and experimental results are in fairly good agreement.

Keywords Wire mesh · Energy · Exergy · Solar air heater · Efficiency · Dual pass

List of symbols

A_c	Area of the collector (m^2)
A_f	Total area of the fins (m^2)
B	Flow channel width (m)
c_p	Specific heat of air (J/kg K)
d_w	Wire diameter of wire mesh (m)
D_h	Hydraulic diameter of the flow channel (m)
e	Artificial roughness height (m)
E	Efficiency increment
H	Flow channel height (m)
h	Heat transfer coefficient (W/m^2 K)
h_b	Conductive heat transfer coefficient across the insulation (W/m^2 K)
I	Incident solar radiation (W/m^2)
k	Thermal conductivity of air (W/m K)
k_i	Thermal conductivity of insulating material (W/m K)
k_s	Thermal conductivity of fin (W/m K)
L	Flow channel length (m)
L_f	Length of the fin (m)
m	Mass flow rate of air (kg/s)
n	Number of wire mesh layer
n_f	Number of the fins
p	Artificial roughness pitch (m)
p_t	Pitch of the wire mesh screen (m)
P	Power consumption increment
P_{wm}	Porosity of packed bed
Q	Energy output of the solar air heater (W)
t	Thickness of the fin (m)
t_i	Thickness of the insulation (m)
T	Average temperature (K)
V	Velocity of air in the channel (m/s)
W_f	Height of the fin (m)

Abbreviations

FPDPSAH	Finned plate dual-pass solar air heater
RPDPSAH	Roughened plate dual-pass solar air heater
SAH	Solar air heater
SPFPSAH	Single-pass flat plate solar air heater
WMDPSAH	Wire mesh dual-pass solar air heater

P. Velmurugan (✉) · R. Kalaivanan
Department of Mechanical Engineering,
Annamalai University, Chennai, Tamilnadu, India
e-mail: pvsrlme@gmail.com

Greek letters

α	Absorptivity
τ	Transmissivity
ε	Emissivity
μ	Dynamic viscosity of air (N s/m^2)
ρ	Density of air (kg/m^3)
η	Energy efficiency (%)
η_f	Fin efficiency (%)
σ	Stefan–Boltzmann constant (W/m^2 K^4)

Subscripts

a	Ambient
ab	Absorber plate
abro	Absorber plate with roughness
c	Convection
c1	Cover-1
c2	Cover-2
f	Fluid
f1	Fluid flow-1
f2	Fluid flow-2
i	Inlet
o	Outlet
r	Radiation
wm	Wire mesh

1 Introduction

Renewable energy sources are extensively used for heating, cooling and drying applications in developing and developed countries owing to rapidly increasing oil prices and increased presence of greenhouse gases [1–3]. Solar air heater (SAH) using air as working medium reduces the number of system components required. Conventional SAHs mainly consist of panel, insulated hot air duct and air blower in dynamic systems. The panel consists of an absorber plate and transparent cover that affects the SAH efficiency. Major heat losses from conventional SAH are found to be top losses, whereas heat losses from the bottom and the sides are negligible owing to adequate insulation. In order to minimize the heat losses and to improve the efficiency, dual glassing was recommended [4,5]. Few researchers suggested the dual-pass mode to decrease the heat losses, enhancement in heat transfer rate and efficiency without increasing the heater size or cost [6–8]. In conventional SAH, the area available for heat transfer is lesser than the projected area of the absorber and becomes unnecessarily hot, leading to higher heat losses [9]. The convective heat transfer rate in flow channel is augmented by increasing the heat transfer surface area and turbulence inside the channel [10–12]. Though the increase in the absorber plate projected area enhances the heat transfer rate, pressure drop across the heater and power consumption also increases [13].

Different modifications were suggested and applied by earlier researchers who employed various design and flow arrangements to enhance the heat transfer rate between the absorber plate and air. Yeh et al. [14] constructed a dual-flow SAH (upper and lower) having similar flow area and mass flow rate, reported better thermal efficiency. Naphon and Kongtragool [15] built analytical models for flat plate SAH with various flow configurations for predicting the heat transfer rate and performance. Sahu and Bhagoria [16] observed augmentation in heat transfer rate while employing transverse ribs on absorber plate. Karim and Hawlader [17] attempted flat plate, finned and v-corrugated absorber plate in single- and dual-pass SAHs analytically and experimentally, who reported a better performance in v-corrugated dual-pass SAH. Ozgen et al. [6] suggested passing the air from above and below the absorber plate at the same time in a dual-flow SAH. The performance investigation of single- and dual-pass SAH with fins and steel wire mesh as absorber was attempted by Omojaro and Aldabbagh [18].

Exergy investigation is a dominant tool in design, optimization and performance evaluation of energy systems [19,20]. Recently, several researchers have undertaken studies covering exergy investigation of SAHs. The energy and exergy efficiencies of various flat plate SAHs were determined by Karsli [21], who opined that solar radiation and construction of SAH dictate the efficiencies. Gupta and Kaushik [22] optimized the performance parameters for achieving maximum exergy delivery in flat plate SAH. Esan [13] experimentally studied the energetic and exergetic efficiencies of dual-flow SAH with and without obstacles under broad variety of operating circumstances.

The objectives of this study were as follows: (1) to analytically and experimentally study the energy and exergy performance of SAHs with various absorber plate geometries at varied mass flow rates and solar intensities and (2) to develop an economically feasible SAH considering efficiency increment and power consumption increment. These objectives were approached through a review of relevant literature, design, construction and testing of various (flat, roughened, finned and wire mesh) SAHs at steady state condition in a solar simulator.

2 Analytical Analysis

The steady state energy balance analysis at various components of the SPFPSAH, RPDPSAH, FPDPSAH and WMDPSAH is attempted for models shown in Figs. 1, 2, 3 and 4, along with the different heat transfer coefficients at their surfaces. The assumptions made are as follows: (1) heat transfer is steady and one-dimensional, (2) heat capacity effects of covers, enclosed air and absorber plate are negligible, (3) temperatures of the absorber plate and fluid flow are func-

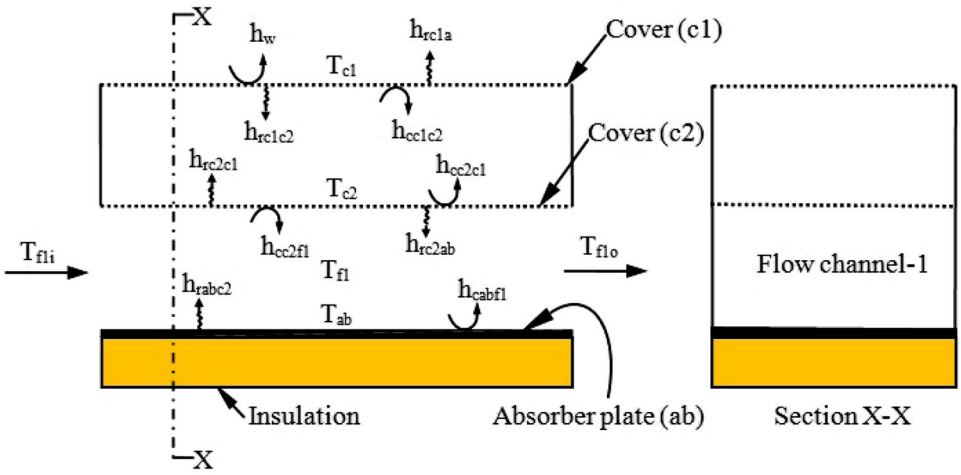

Fig. 1 Single-pass flat plate solar air heater (SPFPSAH)

tions of the flow direction only, (4) there is no air leakage from the flow channel, (5) physical properties of fluid and materials are constant and (6) heat loss from edges of SAHs is considered negligible.

2.1 Energy Balance Equations of SPFPSAH

The energy balance equations for cover-1, cover-2, fluid flow and absorber plate of the SPFPSAH (Fig. 1) can be written as below

Cover-1

$$\alpha_{c1} I = (h_w + h_{rc1a})(T_{c1} - T_a) + (h_{cc1c2} + h_{rc1c2})(T_{c1} - T_{c2}) \quad (1)$$

Cover-2

$$\alpha_{c2}\tau_{c1} I = (h_{rc2c1} + h_{cc2c1})(T_{c2} - T_{c1}) + h_{rc2ab}(T_{c2} - T_{ab}) + h_{cc2f1}(T_{c2} - T_{f1}) \quad (2)$$

Fluid flow-1

$$Q_{f1} = mc_p(T_{f1o} - T_{f1i}) = A_c h_{cc2f1}(T_{c2} - T_{f1}) + A_c h_{cabf1}(T_{ab} - T_{f1}) \quad (3)$$

Absorber plate

$$\alpha_{ab}\tau_{c1}\tau_{c2} I = h_{rabc2}(T_{ab} - T_{c2}) + h_{cabf1}(T_{ab} - T_{f1}) + h_b(T_{ab} - T_a) \quad (4)$$

2.2 Energy Balance Equations of RPDPSAH

The energy balance equations for cover-1, cover-2, first- and second-pass fluid flow, and absorber plate of the RPDPSAH (Fig. 2) can be written as below

Cover-1

$$\alpha_{c1} I = (h_w + h_{rc1a})(T_{c1} - T_a) + h_{rc1c2}(T_{c1} - T_{c2}) + h_{cc1f1}(T_{c1} - T_{f1}) \quad (5)$$

Fluid flow-1

$$Q_{f1} = mc_p(T_{f1o} - T_{f1i}) = A_c h_{cc1f1}(T_{c1} - T_{f1}) + A_c h_{cc2f1}(T_{c2} - T_{f1}) \quad (6)$$

Cover-2

$$\alpha_{c2}\tau_{c1} I = h_{rc2c1}(T_{c2} - T_{c1}) + h_{cc2f1}(T_{c2} - T_{f1}) + h_{rc2ab}(T_{c2} - T_{ab}) + h_{cc2f2}(T_{c2} - T_{f2}) \quad (7)$$

Fluid flow-2

$$Q_{f2} = mc_p(T_{f2o} - T_{f2i}) = A_c h_{cc2f2}(T_{c2} - T_{f2}) + A_c h_{cabrof2}(T_{ab} - T_{f2}) \quad (8)$$

Absorber plate

$$\alpha_{ab}\tau_{c1}\tau_{c2} I = h_{rabc2}(T_{ab} - T_{c2}) + h_{cabrof2}(T_{ab} - T_{f2}) + h_b(T_{ab} - T_a) \quad (9)$$

2.3 Energy Balance Equations of FPDPSAH

The energy balance equations for cover-1, cover-2, first- and second-pass fluid flow, and absorber plate of the FPDPSAH (Fig. 3) can be written as below

Cover-1

$$\alpha_{c1} I = (h_w + h_{rc1a})(T_{c1} - T_a) + h_{rc1c2}(T_{c1} - T_{c2}) + h_{cc1f1}(T_{c1} - T_{f1}) \quad (10)$$

Fluid flow-1

$$Q_{f1} = mc_p(T_{f1o} - T_{f1i}) = A_c h_{cc1f1}(T_{c1} - T_{f1}) + A_c h_{cc2f1}(T_{c2} - T_{f1}) \quad (11)$$

Cover-2

$$\alpha_{c2}\tau_{c1} I = h_{rc2c1}(T_{c2} - T_{c1}) + h_{cc2f1}(T_{c2} - T_{f1}) + h_{rc2ab}(T_{c2} - T_{ab}) + h_{cc2f2}(T_{c2} - T_{f2}) \quad (12)$$

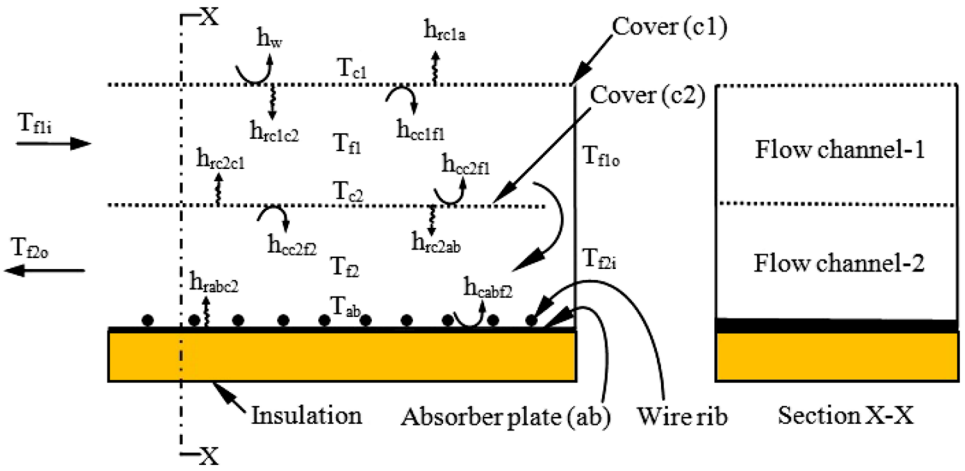

Fig. 2 Roughened plate dual-pass solar air heater (RPDPSAH)

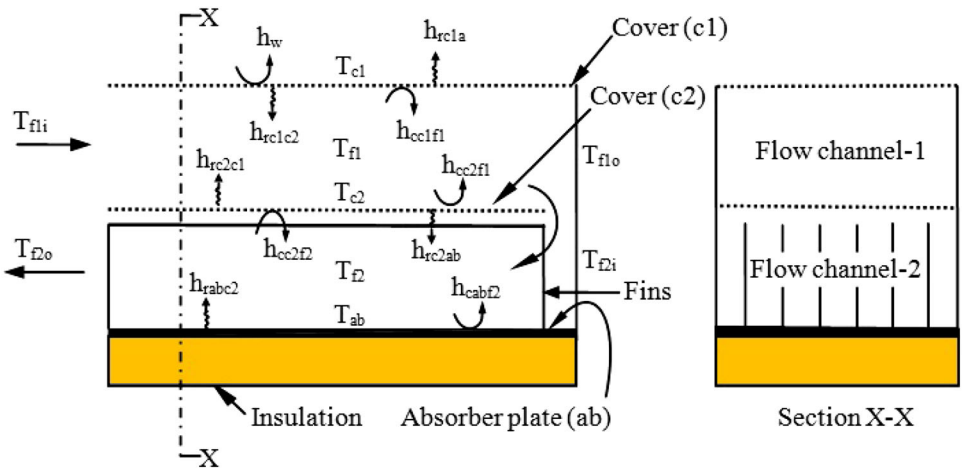

Fig. 3 Finned plate dual-pass solar air heater (FPDPSAH)

Fluid flow-2

$$Q_{f2} = mc_p\,(T_{f2o} - T_{f2i}) = A_c h_{cc2f2}\,(T_{c2} - T_{f2}) + A_c h_{cabf2}\phi\,(T_{ab} - T_{f2}) \quad (13)$$

Absorber plate

$$\alpha_{ab}\tau_{c1}\tau_{c2} I = h_{rabc2}\,(T_{ab} - T_{c2}) + h_{cabf2}\phi\,(T_{ab} - T_{f2}) + h_b\,(T_{ab} - T_a) \quad (14)$$

where the dimensionless quantity ϕ and fin efficiency η_f are defined with collector surface area A_c and total surface area of fins A_f *as*

$$\phi = 1 + (A_f/A_c)\,\eta_f \quad (15)$$

$$A_f = 2n_f W_f L_f \quad (16)$$

$$\eta_f = \tanh(MW_f)/MW_f \quad (17)$$

$$M = \sqrt{2h_{cabf}/k_s t} \quad (18)$$

2.4 Energy Balance Equations of WMDPSAH

The energy balance equations for cover-1, cover-2, first and second pass fluid flow, and absorber plate of the WMDPSAH (Fig. 4) can be written as below

Cover-1

$$\alpha_{c1} I = (h_w + h_{rc1a})\,(T_{c1} - T_a) + h_{rc1c2}\,(T_{c1} - T_{c2}) + h_{cc1f1}\,(T_{c1} - T_{f1}) \quad (19)$$

Fluid flow-1

$$Q_{f1} = mc_p\,(T_{f1o} - T_{f1i}) = A_c h_{cc1f1}\,(T_{c1} - T_{f1}) + A_c h_{cc2f1}\,(T_{c2} - T_{f1}) \quad (20)$$

Cover-2

$$\alpha_{c2}\tau_{c1} I = h_{rc2c1}\,(T_{c2} - T_{c1}) + h_{cc2f1}\,(T_{c2} - T_{f1}) + h_{rc2ab}\,(T_{c2} - T_{ab}) + h_{cc2f2}\,(T_{c2} - T_{f2}) \quad (21)$$

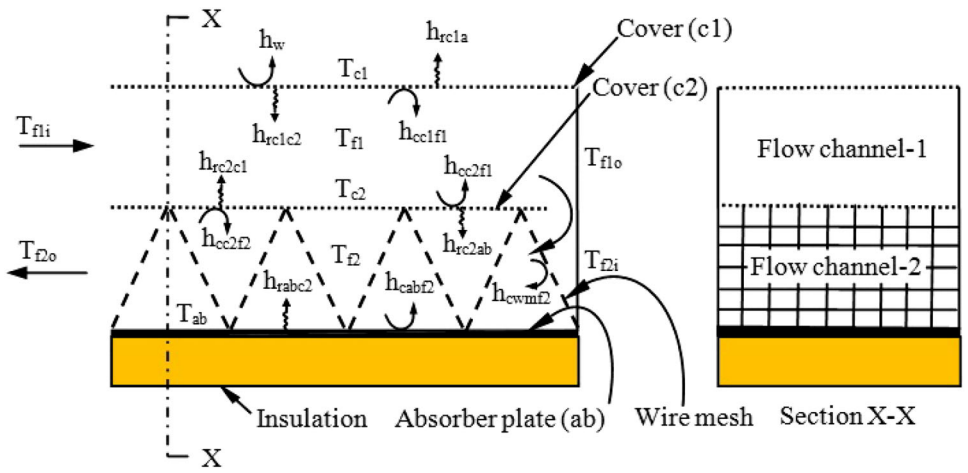

Fig. 4 Wire mesh dual-pass solar air heater (WMDPSAH)

Fluid flow-2

$$Q_{f2} = mc_p\,(T_{f2o} - T_{f2i}) = A_c h_{cc2f2}\,(T_{c2} - T_{f2}) + A_c h_{cabf2}\,(T_{ab} - T_{f2}) + A_{wm} h_{cwmf2}\,(T_{wm} - T_{f2}) \quad (22)$$

Absorber plate

$$\alpha_{ab}\tau_{c1}\tau_{c2} I = h_{rabc2}\,(T_{ab} - T_{c2}) + h_{cabf2}\,(T_{ab} - T_{f2}) + h_b\,(T_{ab} - T_a) \quad (23)$$

2.5 Heat Transfer Coefficient and Pressure Drop

The convective heat transfer coefficient (h_w) from the cover-1 to the ambience is calculated by the following expression [23] to be valid for a wind speed range $0 \le V_w < 5$ m/s

$$h_w = 5.7 + 3.8\,V_w \quad (24)$$

where V_w is wind velocity of the ambient air (m/s).

The radiation heat transfer coefficient (h_{rc1a}) from the cover-1 to ambience is obtained as

$$h_{rc1a} = \sigma\varepsilon_{c1}\left(T_{c1}^2 + T_a^2\right)(T_{c1} + T_a) \quad (25)$$

The radiative heat transfer coefficients between the absorber plate and cover-2 (h_{rabc2}) and between cover-1 and cover-2 (h_{rc1c2}) are calculated by the formula of two infinite parallel plates (i, j):

$$h_{rij} = \sigma\left(T_i + T_j\right)\left(T_i^2 + T_j^2\right)/\left(1/\varepsilon_i + 1/\varepsilon_j - 1\right) \quad (26)$$

where ε_i and ε_j are the emissivities of the two surfaces.

The conduction heat transfer coefficient (h_b) across the insulation (assuming convection and radiation resistances from bottom surface of insulation are negligible) is given by [24]

$$h_b = k_i/t_i \quad (27)$$

Due to stagnated air prevailing in enclosure for parallel plate between cover-1 and cover-2, natural convection heat transfer coefficient (h_{cc1c2}) for SPFPSAH is determined by [24]

$$h_{cc1c2} = 1.25\,(T_{c2} - T_{c1})^{0.25} \quad (28)$$

The forced convection heat transfer coefficient for the fluid moving on the cover-2 and absorber plate is calculated by [25]

$$h_{cc2f} = h_{cabf} = (k/D_h)\,0.018\;Re^{0.8}\;Pr^{0.4} \quad (29)$$

where

$$D_h = 4HB/2\,(H + B) \quad (30)$$

The convective heat transfer coefficient (h_{cabrof}) between roughened surface and fluid is estimated by the following correlation [26]

$$h_{cabrof} = (k/D_h)\,0.08596\,(p/e)^{-0.054}\,(e/D_h)^{0.072}\;Re^{0.723} \quad (31)$$

where Re is the Reynolds number, defined as

$$Re = 2m/\mu\,(B + H) \quad (32)$$

The convective heat transfer coefficient (h_{cwmf}) between wire mesh and fluid is evaluated by [27]

$$h_{cwmf} = \left(J_h c_p G_o\right)/Pr^{2/3} \quad (33)$$

where

$$J_h = 0.647\left[\frac{1}{nP_{wm}}\left(p_t/d_w\right)\right]^{2.104} Re_p^{-0.55} \quad (34)$$

where Re_p is the Reynolds number for the wire mesh channel and is estimated by

$$Re_p = 4r_h G_o/\mu \quad (35)$$

where r_h and G_o are the hydraulic radius for the wire mesh channel and mass velocity of air, respectively, calculated by

$$r_h = P_{wm}d_w/4\,(1 - P_{wm}),\;\; G_o = m/A_{cs}P_{wm} \quad (36)$$

The total pressure drop (ΔP) across the SAH is determined by

$$\Delta P = \Delta P_{\text{channel}} + \Delta P_{\text{bend}} \tag{37}$$

The pressure drop ($\Delta P_{\text{channel}}$) across the flow channel is estimated as

$$\Delta P_{\text{channel}} = 2\rho f L V^2 / D_h \tag{38}$$

where f is the friction factor in the channel with fins attached to the absorber plate for turbulent flow and is calculated by [28]

$$f = 0.079\ Re^{-0.25} \tag{39}$$

Roughened surface friction factor (f_{ro}) is estimated by the following correlation [26]

$$f_{\text{ro}} = 0.245\,(p/e)^{-0.206}\,(e/D_h)^{0.243}\ \ Re^{-1.25} \tag{40}$$

The pressure drop across ($\Delta P_{\text{channel}}$) the wire mesh channel can be determined from the following expression

$$\Delta P_{\text{channel}} = f_{\text{wm}} L \rho V^2 / 2 r_h \tag{41}$$

where friction factor in wire mesh (f_{wm}) is calculated by the following correlation [27]

$$f_{\text{wm}} = 2.484 \left[\frac{1}{n P_{\text{wm}}}\left(p_t / d_{\text{w}}\right)\right]^{0.699}\ \ Re_{\text{p}}^{-0.44} \tag{42}$$

The pressure drop (ΔP_{bend}) for the 180° close return bend may be calculated as

$$\Delta P_{\text{bend}} = K \rho V^2 / 2 \tag{43}$$

where K is the coefficient and has the value of 2.2 [29] for the 180° close return bend.

2.6 Energy Analysis

The following expression is applied to evaluate the energy output (Q) of the SAH [30]

$$Q = m c_{\text{p}}\,(T_{\text{fo}} - T_{\text{fi}}) \tag{44}$$

The energy efficiency (η) of the SAH is determined by

$$\eta = Q / A_{\text{c}} I \tag{45}$$

2.7 Exergy Analysis

In the exergy analysis, pressure drop is considered, treating air as perfect gas, kinetic and potential energy changes are negligible, and the process is steady state and steady flow. Figure 5 schematically shows the exergy flows in the SAH. The general exergy balance can be expressed as [31]

$$\begin{aligned} Ir &= Ex_{\text{dest}} = Ex_{\text{loss}} = Ex_{\text{in}} - (Ex_{\text{fo}} - Ex_{\text{fi}}) \\ &= Ex_{\text{in}} - Ex_{\text{out}} \end{aligned} \tag{46}$$

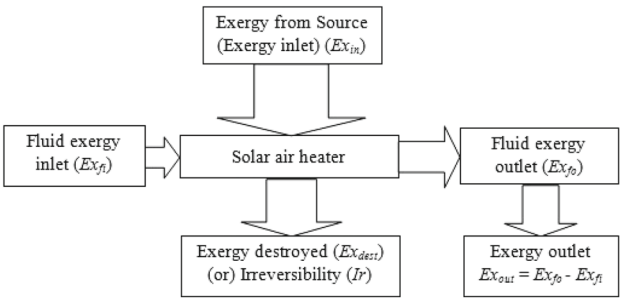

Fig. 5 Exergy flows in a solar air heater

where Ex_{in} is the exergy supplied to the SAH obtained by [32]

$$Ex_{\text{in}} = (1 - (T_{\text{fi}}/T_s))\ Q_{\text{s}} \tag{47}$$

where T_{s} is the source temperature (K) and Q_{s} is the total rate of the energy received by the absorber plate from the source evaluated by [31]

$$Q_{\text{s}} = \alpha_{\text{ab}} \tau_{\text{c1}} \tau_{\text{c2}} I A_{\text{c}} \tag{48}$$

Exergy output (Ex_{out}) of the SAH can be calculated by [33]

$$\begin{aligned} Ex_{\text{out}} &= m c_{\text{p}}\,(T_{\text{fo}} - T_{\text{fi}} - T_{\text{a}} \ln (T_{\text{fo}}/T_{\text{fi}})) \\ &\quad - (m/\rho)\,\Delta P\,(T_a/T_{\text{fm}}) \end{aligned} \tag{49}$$

where T_{fm} is mean air temperature of inlet and outlet (°C).

From Eqs. 46–49, the rate of irreversibility (Ir) in SAH is obtained as

$$\begin{aligned} Ir &= (1 - (T_{\text{fi}}/T_s))\ Q_{\text{s}} - m c_{\text{p}}\,(T_{\text{fo}} - T_{\text{fi}} - T_{\text{a}} \ln (T_{\text{fo}}/T_{\text{fi}})) \\ &\quad - (m/\rho)\,\Delta P\,(T_{\text{a}}/T_{\text{fm}}) \end{aligned} \tag{50}$$

The exergy efficiency (or) second law efficiency (η_{ex}) can be obtained as

$$\eta_{\text{ex}} = Ex_{\text{out}} / Ex_{\text{in}} \tag{51}$$

2.8 Analytical Calculation

In order to evaluate analytical value of energy and exergy efficiency of various types of SAHs at different mass flow rates and solar intensities, numerical calculations are performed using collector configuration, system properties and operating conditions. The works reporting numerical techniques for determining the cover temperatures (T_{c1} and T_{c2}), absorber plate temperature (T_{ab}) and fluid flow temperatures (T_{f1} and T_{f2}) are sparse. In the present work, the component temperatures above the ambient temperature are initially chosen in order to determine the various heat transfer coefficients using Eqs. 24–34, upon which all the above parameters depend on and subsequently the new temperatures of various components are determined by Gauss Seidel

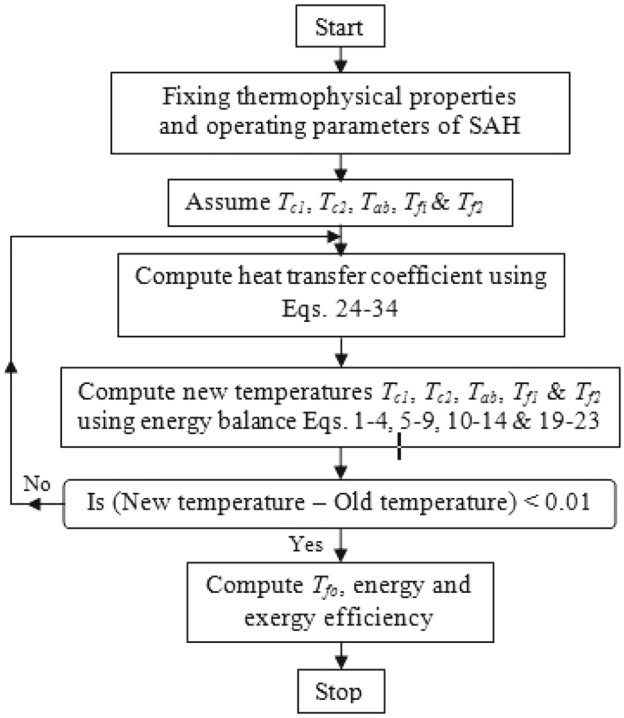

Fig. 6 Flow chart of the program

iteration method using energy balance Eqs. 1–4 (for SPFPSAH), Eqs. 5–9 (for RPDPSAH), Eqs. 10–14 (for FPDPSAH) and Eqs. 19–23 (for WMDPSAH). The flow chart of the executed MATLAB program to obtain various parameters is shown in Fig. 6. If the new temperatures differ more than 0.01 % from their respective initial values, then the new temperatures will be used as the assumed temperatures for the next iteration and the process is repeated until an optimum new temperature is obtained within ±0.01 % deviation of their respective input values. In order to obtain the energy efficiency (Eq. 45) and exergy efficiency (Eq. 51) numerically, codes are developed in MATLAB 8.1 using following operating and geometries parameters of SAH: $t_i = 0.05$ m, $k_i = 0.025$ W/m K, $\varepsilon_{ab} = 0.94$, $\varepsilon_b = 0.94$, $\varepsilon_{c1} = 0.9$, $\varepsilon_{c2} = 0.9$, $\alpha_{ab} = 0.95$, $\alpha_{c1} = 0.06$, $\alpha_{c2} = 0.06$, $\tau_{c1} = 0.84$, $\tau_{c2} = 0.84$, $I = 500, 550$ & 600 W/m^2, $m = 0.01, 0.02, 0.03$ & 0.04 kg/s, $L = 2$ m, $B = 0.46$ m, $H = 0.025$ m, $\sigma = 5.67 \times 10^{-8}$ W/m^2 K^4, $V_w = 1.5$ m/s, $t = 0.00095$ m, $n_f = 17$, $L_f = 1.98$ m, $k_s = 50.2$ W/m K, $W_f = 0.025$ m, $d_w = 0.0003$ m, $e = 0.0015$ m, $p = 0.015$ m, $P_{wm} = 0.9953$, $p_t = 0.0025$ m.

3 Experimental Setup and Procedure

The top plane of the collector (glass cover) is uniformly heated by an incident radiation using solar simulator. An indoor solar simulator test facility is photographically and schematically shown in Figs. 7 and 8, respectively. In solar

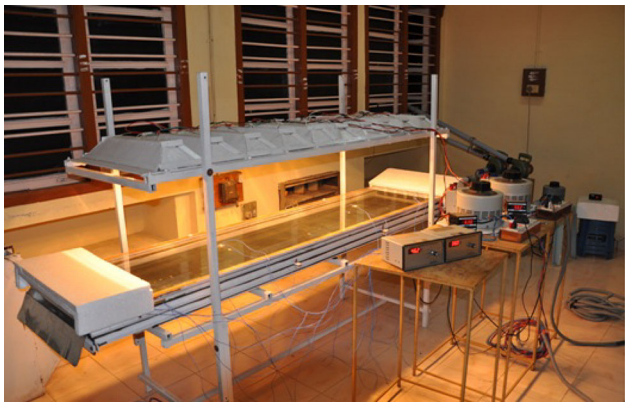

Fig. 7 Photographic view of experimental setup

simulator, 20 halogen bulbs (each 300 W) are fixed on a frame having similar area of the collector, placed 1 m above the glass cover such that the utmost average radiation of 645 W/m^2 is attained at full load conditions. During experimentation, incident radiation was adjusted by the input power to the bulbs, being controlled by two AC variacs (4.5 kW each). The incident radiation was measured at the surface of the glass cover by using solarimeter (KIMO SL-100) calibrated by a standard pyranometer.

The single-pass flat plate and dual-pass SAHs with roughness, fins and wire mesh are schematically illustrated in Figs. 1 and 2, 3 and 4, respectively. In single-pass SAH, air passes between absorber plate and cover-2, whereas in dual-pass SAH, air passes between cover-1 and cover-2 and then flows between the absorber plate and cover-2. The SAHs consist of the two glass covers, absorber plate and an insulated container. Normal window glass (4 mm thickness) was used as glazing, and the absorbers were constructed using black-painted low carbon steel. The dimensions of all the SAH absorber plates were maintained as 2 m, 0.46 m and 1 mm (length, width and thickness, respectively). Roughened absorber surface was fabricated with a mild steel wire of diameter (e) 1.5 mm and pitch (p) 15 mm (Fig. 9a). Finned absorber surface is fabricated with 17 longitudinal fins made of mild steel whose dimensions are 1.98, 0.025 and 0.001 m (length, height and thickness), respectively (Fig. 9b). Distance between the two adjacent fins is 0.025 m. Steel wire mesh (0.3 mm diameter) consists of 2.5 mm × 2.5 mm in cross-sectional opening. Single layer wire mesh painted with black is assembled in a transverse v-corrugated shape whose angle and height are 60° and 2.5 cm, respectively (Fig. 9c). The depth of each flow channel of SAHs is 2.5 cm and wrapped with polystyrene to curtail the losses to the ambience.

A variable speed centrifugal blower, capable of delivering a 180 m^3/h, is employed to suck the air through the SAH. The flow rate was maintained by varying the blower speed using AC variac (1.5 kW). Forced convection was generated

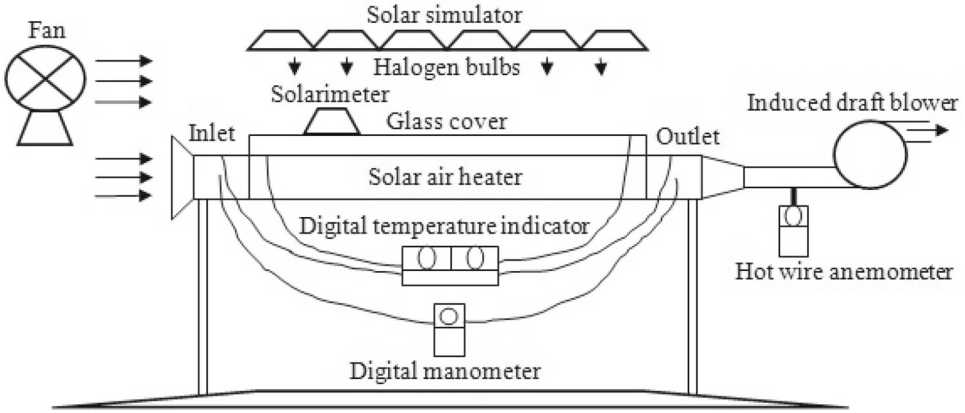

Fig. 8 Schematic line diagram of the experimental setup with solar simulator

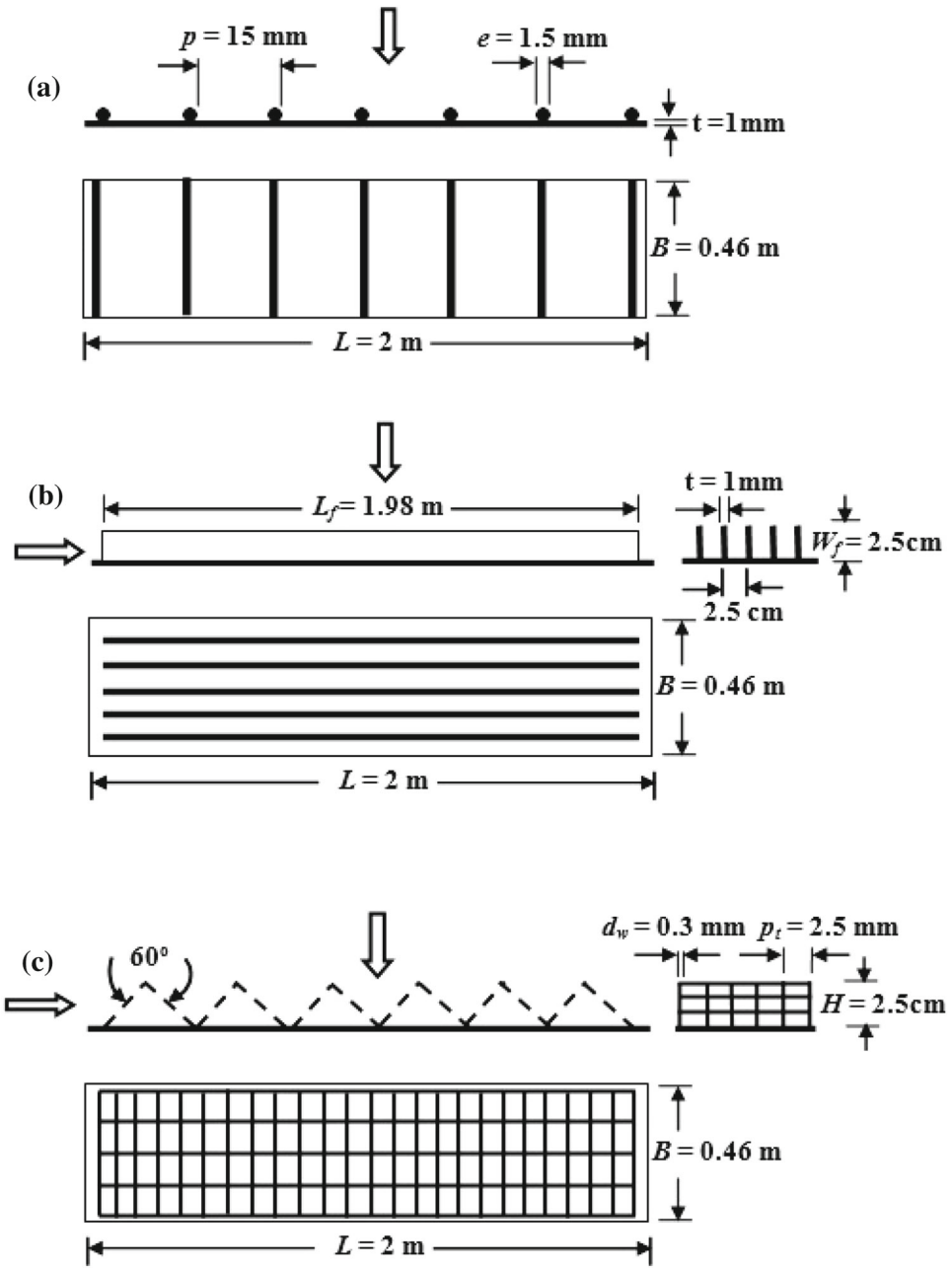

Fig. 9 Schematic diagram of various absorber plate configurations

around the SAH with a velocity of 1.5 m/s by an electrical fan (60 W). The absorber plate temperature and inlet and outlet temperatures of air are measured employing calibrated copper–constantan thermocouples (T-type) with digital temperature indicator. The velocity of flowing air is measured by hot wire anemometer (KIMO VT100), and the pressure drop across the SAH was measured by digital manometer (HT-1891). The steady state inlet and outlet temperatures of air and absorber plate temperatures were noted. The mass flow rate and solar intensity of SAH were varied from 0.01 to 0.04 kg/s and 500 to 600 W/m^2, respectively, and the results are reported.

4 Uncertainty Analysis

Uncertainty analysis is a dominant tool, in planning and design of experiments. An uncertainty estimated quantity, Y depends on independent variables such as $x_1, x_2 \ldots x_n$. The errors in the independent variables are $(\partial x_1/x_1)$, $(\partial x_2/x_2) \ldots (\partial x_n/x_n)$, and then, the uncertainty of dependent variable Y is calculated by [17]

$$\partial Y/Y = \left[(\partial x_1/x)^2 + (\partial x_2/x_2)^2 \ldots (\partial x_n/x_n)^2\right]^{0.5} \quad (52)$$

The maximum possible errors in various measured independent variables, namely inlet and outlet temperatures of air, velocity of air, solar intensity and pressure in the channel, are estimated from the maximum values of output and accuracy of the instrument. In this study, accuracy of instruments, viz. T-type thermocouple 0.1 °C, hot wire anemometer ±3 %, digital manometer ±0.3 % and solarimeter ±1 %, was used. From the above measured independent variables, energy efficiency and mass flow rate were calculated. Equation for energy efficiency is

$$\eta = mc_\mathrm{p}\,(T_\mathrm{fo} - T_\mathrm{fi})/A_\mathrm{c} I \quad (53)$$

In Eq. 53, if A_c and c_p are considered constants, Eq. 53 is modified as

$$\eta = f(T_\mathrm{fo}, T_\mathrm{fi}, I, m) \quad (54)$$

Equation for mass flow rate is

$$m = \rho A V \quad (55)$$

As density of air ρ is dependent on pressure p_r and temperature T, following relationship can be estimated

$$m = f(V, T, p_\mathrm{r}) \quad (56)$$

From Eq. 52, the uncertainty of mass flow rate can be obtained as

$$\partial m/m = \left[(\partial p_\mathrm{r}/p_\mathrm{r})^2 + (\partial V/V)^2 + (\partial T/T)^2\right]^{0.5} \quad (57)$$

Similarly, the uncertainty of energy efficiency can be written as

$$\partial \eta/\eta = \left[(\partial m/m)^2 + (\partial T_\mathrm{fo}/T_\mathrm{fo})^2 + (\partial T_\mathrm{fi}/T_\mathrm{fi})^2 + (\partial I/I)^2\right]^{0.5} \quad (58)$$

The uncertainties of dependent variables, viz. mass flow rate of air and energy efficiency, were calculated by Eqs. 57 and 58, respectively. Using these equations, estimated uncertainty values of mass flow rate and energy efficiency were ±3.18 % and ±3.55 %, respectively.

5 Statistical Analysis

The root mean square percent deviation (q) is evaluated to compare the analytical and experimental results, using the following expressions [34]

$$q = \sqrt{\Sigma\,(q_i)^2/N} \quad (59)$$

$$q_i = [(E_i - F_i)/E_i] \times 100 \quad (60)$$

where E_i is the experimental data, F_i is the theoretical data, and N is the number of experiments.

6 Relative Energy Efficiency Increment

The relative efficiency increment of RPDPSAH (E_RPDPSAH), FPDPSAH (E_FPDPSAH) and WMDPSAH (E_WMDPSAH) is defined relative to SPFPSAH as [35]

$$E_\mathrm{RPDPSAH} = (\eta_\mathrm{RPDPSAH} - \eta_\mathrm{SPFPSAH})/\eta_\mathrm{SPFPSAH} \quad (61)$$

$$E_\mathrm{FPDPSAH} = (\eta_\mathrm{FPDPSAH} - \eta_\mathrm{SPFPSAH})/\eta_\mathrm{SPFPSAH} \quad (62)$$

$$E_\mathrm{WMDPSAH} = (\eta_\mathrm{WMDPSAH} - \eta_\mathrm{SPFPSAH})/\eta_\mathrm{SPFPSAH} \quad (63)$$

in which η_SPFPSAH, η_RPDPSAH, η_FPDPSAH and η_WMDPSAH denote the energy efficiencies of SPFPSAH, RPDPSAH, FPDPSAH and WMDPSAH, respectively.

7 Relative Power Consumption Increment

The necessary instantaneous fan power required (U) for forcing a certain rate of air through the SAH is calculated by [36]

$$U = F_\mathrm{flow}/\eta_\mathrm{fan}\eta_\mathrm{motor} \quad (64)$$

where η_fan and η_motor are fan and motor efficiencies, respectively

The pumping power (F_flow) is estimated by the following relation [28]

$$F_\mathrm{flow} = m\Delta P/\rho \quad (65)$$

The relative power consumption increment of RPDPSAH (P_RPDPSAH), FPDPSAH (P_FPDPSAH) and WMDPSAH (P_WMDPSAH) is defined with respect to SPFPSAH as [24]

$$P_{\mathrm{RPDPSAH}} = (U_{\mathrm{RPDPSAH}} - U_{\mathrm{SPFPSAH}})/U_{\mathrm{SPFPSAH}} \quad (66)$$

$$P_{\mathrm{FPDPSAH}} = (U_{\mathrm{FPDPSAH}} - U_{\mathrm{SPFPSAH}})/U_{\mathrm{SPFPSAH}} \quad (67)$$

$$P_{\mathrm{WMDPSAH}} = (U_{\mathrm{WMDPSAH}} - U_{\mathrm{SPFPSAH}})/U_{\mathrm{SPFPSAH}} \quad (68)$$

where U_{SPFPSAH}, U_{RPDPSAH}, U_{FPDPSAH} and U_{WMDPSAH} represent the power consumption for SPFPSAH, RPDPSAH, FPDPSAH and WMDPSAH, respectively.

8 Results and Discussion

The energy and exergy performance of the SPFPSAH, RPDPSAH, FPDPSAH and WMDPSAH was investigated analytically and experimentally at constant wind velocity ($V_w = 1.5$ m/s), varied mass flow rate (0.01–0.04 kg/s) and solar intensities (500–600 W/m^2). Figure 10 shows the temperature rise of air versus mass flow rate of air for WMDPSAH, FPDPSAH, RPDPSAH and SPFPSAH. The temperature rise of air decreases with mass flow rate of air for all attempted SAHs and is consistent with Velmurugan and Kalaivanan [31]. The heat removal capacity of air enhances with mass flow rate and consequently absorber plate temperature decreases. As seen from the Fig. 10, the temperature rise of air of WMDPSAH (both enhanced turbulence and heat transfer area) is higher than that of FPDPSAH (enhanced heat transfer area), than that of RPDPSAH (enhanced turbulence) and also than that of SPFPSAH (without enhanced turbulence and heat transfer area). Augmented turbulence and heat transfer area contribute to the higher temperature rise of air for WMDPSAH. Moreover, the temperature rise of air for dual-pass SAHs is higher than single-pass SAH due to the preheating of the air through the first pass and then reheating in the second pass. The highest temperature rise of air obtained in this study is 25.2 °C for WMDPSAH at $m = 0.01$ kg/s.

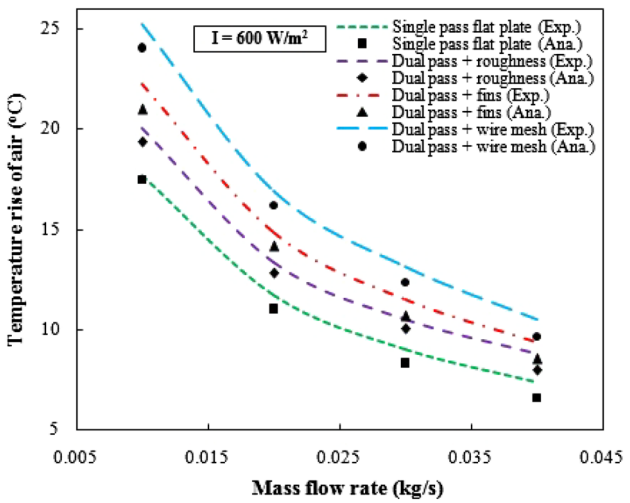

Fig. 10 Variation of temperature rise of air with mass flow rate

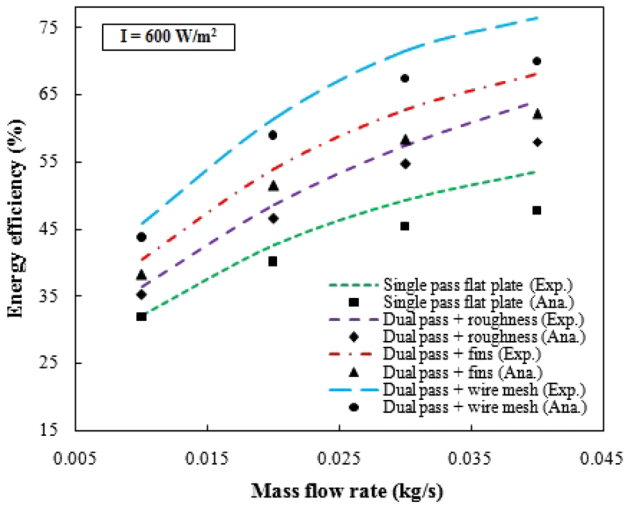

Fig. 11 Variation of energy efficiency with mass flow rate

Figure 11 shows the variation of energy efficiency with mass flow rate for WMDPSAH, FPDPSAH, RPDPSAH and SPFPSAH. Experimental result shows that energy efficiency of all four SAHs increases with mass flow rate as the heat transfer rate between absorber plate and flowing air is more and reduced energy losses to ambience as reported by Karim and Hawlader [17]. It is clear from Fig. 11 that the WMDPSAH is more efficient than FPDPSAH, RPDPSAH and SPFPSAH. Experimental results proved that WMDPSAH is 13.71–22.86 %, 9.47–12.37 % and 5.44–8.29 % more efficient than SPFPSAH, RPDPSAH and FPDPSAH, respectively. The introduction of wire mesh in WMDPSAH increases the effective heat transfer area per unit volume of packed (wire mesh) channel, and therefore, the volumetric heat transfer coefficient between wire mesh and air increases to result in higher energy efficiency. Further, in WMDPSAH, not only the absorber plate but also the wire mesh works as the absorber of solar radiation. Therefore, the heat energy due to absorption of solar radiation is distributed over the wire mesh and absorber plate, which is dissipated more effectively to the flowing fluid on account of very large surface area compared with FPDPSAH, RPDPSAH and SPFPSAH. In addition, the dual-pass SAHs energy efficiencies are higher than single-pass SAH following the reduction in the heat losses from the top cover (preheating of air). Due to the above reasons, energy efficiency in case of packed (wire mesh) SAH is better than other variants. In this study, maximum energy efficiency of 76.46 % is obtained at $m = 0.04$ kg/s for WMDPSAH. The statistical expressions for efficiencies of SPFPSAH, RPDPSAH, FPDPSAH and WMDPSAH are determined using linear regression statistical technique employing least square fitting of the experimental data given by

$$\eta_{\mathrm{SPFPSAH}} = 710.2X + 26.67 \quad (69)$$

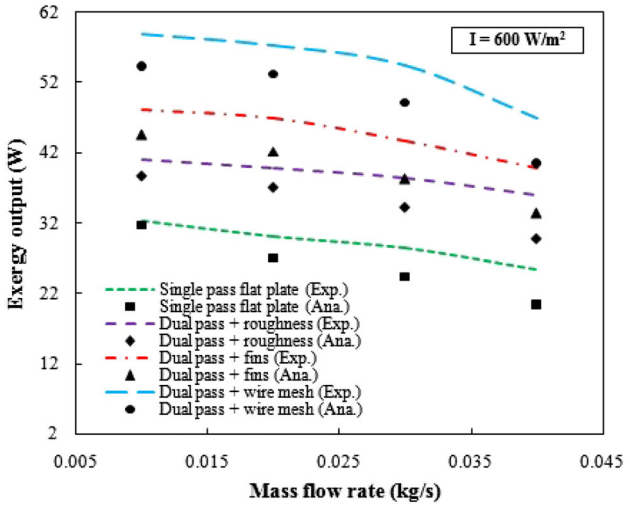

Fig. 12 Variation of exergy output with mass flow rate

$$\eta_{\text{RPDPSAH}} = 919.7X + 28.63 \quad (70)$$

$$\eta_{\text{FPDPSAH}} = 920.4X + 33.31 \quad (71)$$

$$\eta_{\text{WMDPSAH}} = 1017.2X + 38.43 \quad (72)$$

It is observed from Figs. 10 and 11 that analytical and experimental values are in fairly good agreement with each other. The root mean square percent deviations (Eq. 59) between analytical and experimental results are 7.4 % (for SPFPSAH), 6.7 % (for RPDPSAH), 6.6 % (for FPDPSAH) and 6.1 % (for WMDPSAH). The deviations between experimental and analytical results are due to uncertainties in the correlations used in calculating various heat transfer coefficients. Heat capacities of glass covers and absorber plate are not considered in the analytical analysis this being another source for deviation.

From Fig. 12, it is evident that the exergy output decreases with mass flow rate for all SAHs as the temperature rise of air is lower at higher mass flow and is consistent with Sun et al. [33]. The maximum exergy output for SPFPSAH, RPDPSAH, FPDPSAH and WMDPSAH is determined as 32.27, 40.96, 48.04 and 58.82 W, at $m = 0.01$ kg/s. Gupta and Kaushik [22] proved that the maximum exergy output is achieved at lower mass flow rate. WMDPSAH yields higher exergy output for all mass flow rates (Fig. 12) than FPDPSAH, RPDPSAH and SPFPSAH following more quality of energy transfer between absorber plate and air. The root mean square percent deviations (Eq. 59) between analytical and experimental results of exergy output are 13.5 % (for SPFPSAH), 12.3 % (for RPDPSAH), 11.9 % (for FPDPSAH) and 9.9 % (for WMDPSAH).

When the mass flow rate is increased, energy efficiency increases, while the second law efficiency decreases for WMDPSAH, FPDPSAH, RPDPSAH and SPFPSAH (Fig. 11; Table 1). Second law efficiencies were observed to be maximum at lower mass flow rate ($m = 0.01$ kg/s), whereas energy efficiencies reach maximum value at higher mass flow rate ($m = 0.04$ kg/s) due to quality of energy transfer is higher at lower mass flow rate and quantity of energy transfer is maximum at higher mass flow rate. Further, the

Table 1 Exergy analysis of SAHs with varied geometries at $I = 600\,\text{W/m}^2$

Solar air heaters	Mass flow rate (kg/s)	Exergy inlet (Ex_{in}) (W)		Exergy outlet (Ex_{out}) (W)		Irreversibility (Ex_{dest}) (W)		Exergy loss (%)		Second law efficiency (%)	
		Exp.	Ana.	Exp.	Ana.	Exp.	Ana.	Exp.	Ana.	Exp.	Ana.
FPSPSAH	0.01	257.8	257.8	32.3	31.6	225.5	226.2	87.48	87.75	12.52	12.25
	0.02	257.5	257.5	30.1	26.9	227.4	230.6	88.30	89.54	11.70	10.46
	0.03	257.8	257.8	28.5	24.3	229.4	233.5	88.96	90.56	11.04	9.44
	0.04	257.6	257.6	25.5	20.3	232.2	237.4	90.12	92.11	9.88	7.89
RPDPSAH	0.01	258.2	258.2	40.9	38.6	217.2	219.6	84.14	85.04	15.86	14.96
	0.02	258.2	258.2	39.7	36.9	218.5	221.2	84.62	85.68	15.38	14.32
	0.03	258.3	258.3	38.5	34.2	219.7	223.9	85.10	86.74	14.90	13.26
	0.04	258.1	258.1	36.1	29.7	222.1	228.3	86.05	88.48	13.95	11.52
FPDPSAH	0.01	257.7	257.7	48.1	44.5	209.7	213.2	81.36	82.73	18.64	17.27
	0.02	257.8	257.8	46.8	42.3	210.9	215.5	81.83	83.61	18.17	16.39
	0.03	257.8	257.8	43.7	38.2	214.1	219.6	83.03	85.17	16.97	14.83
	0.04	257.9	257.9	39.7	33.3	218.1	224.5	84.58	87.07	15.42	12.93
WMDPSAH	0.01	257.5	257.5	58.8	54.2	198.7	203.3	77.16	78.94	22.84	21.03
	0.02	257.3	257.3	57.3	53.2	200.1	204.1	77.74	79.34	22.26	20.66
	0.03	257.4	257.4	54.5	49.1	202.9	208.4	78.83	80.93	21.17	19.07
	0.04	257.5	257.5	46.8	40.5	210.6	217.1	81.80	84.29	18.20	15.71

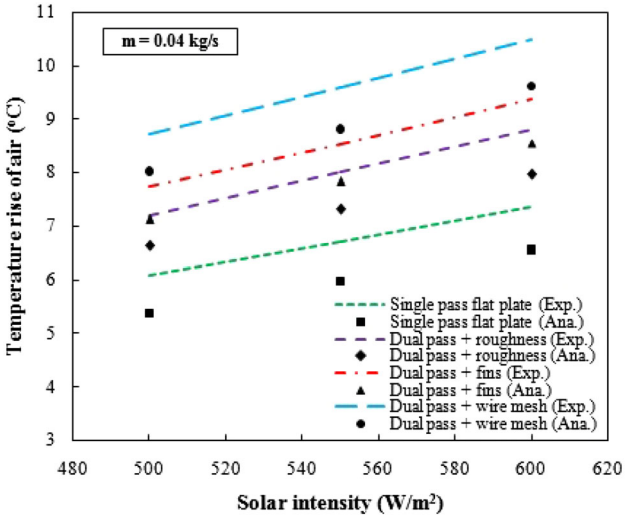

Fig. 13 Variation of temperature rise of air with solar intensity

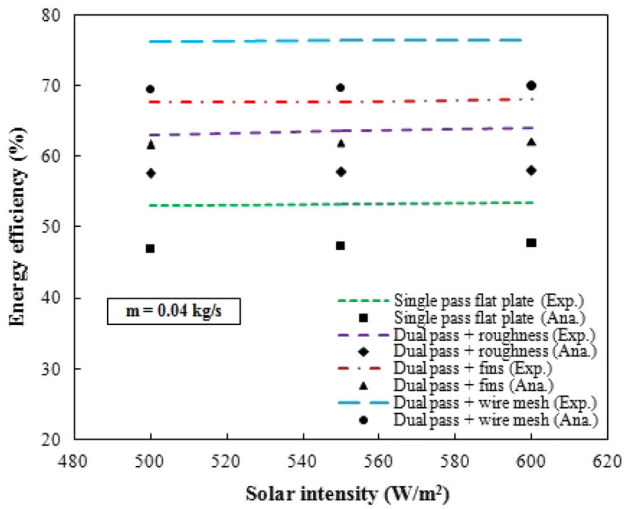

Fig. 14 Variation of energy efficiency with solar intensity

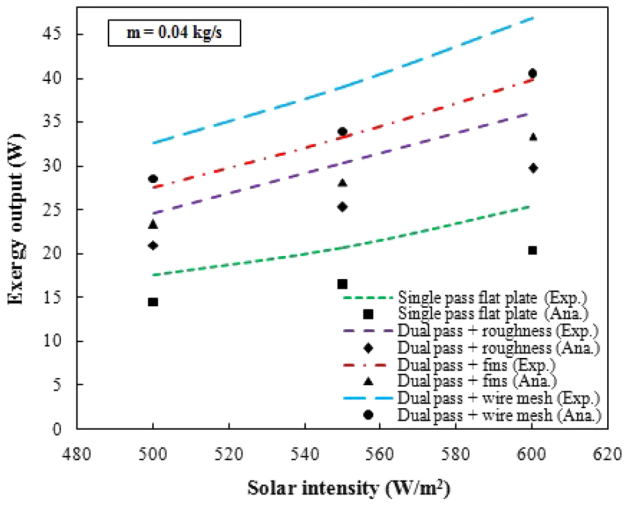

Fig. 15 Variation of exergy output with solar intensity

analytical and experimental exergy loss or irreversibility of WMDPSAH is lower than FPDPSAH, RPDPSAH and SPFPSAH for all attempted mass flow rates (Table 1).

Figure 13 shows that the temperature rise of air increases with radiation intensity for all SAHs. It is evident that the WMDPSAH is more effective in increasing the temperature rise of air compared with SPFPSAH, RPDPSAH and FPDPSAH at all solar intensities owing to more efficient absorption of radiation and heat transfer between absorbing surface and air inside the WMDPSAH. Figure 14 compares the analytical and experimental energy efficiency for SPFPSAH, RPDPSAH, FPDPSAH and WMDPSAH at varied solar intensity (I = 500–600 W/m^2). WMDPSAH exhibits better energy efficiency than SPFPSAH, RPDPSAH and FPDPSAH at different solar intensities. Also, it can be seen that radiation intensity has tiny effect on the energy efficiencies of all SAHs considered in this study. The root mean square percent deviations (Eq. 59) between analytical and experimental results of temperature rise of air and energy efficiency are 11.2 % (for SPFPSAH), 8.6 % (for RPDPSAH), 8.3 % (for FPDPSAH) and 8.2 % (for WMDPSAH).

Figure 15 shows the influence of solar intensity on the exergy output for SPFPSAH, RPDPSAH, FPDPSAH and WMDPSAH. It was revealed from Fig. 15 that the exergy output increases with solar intensity for all conditions owing to increase in the absorber plate temperature and consequently, higher the quality of energy transfer to the air. WMDPSAH exhibits more exergy output than SPFPSAH, RPDPSAH and FPDPSAH for all solar intensities (Fig. 15). The root mean square percent deviations (Eq. 59) between analytical and experimental results of exergy output are 14.8 % (for SPFPSAH), 15.1 % (for RPDPSAH), 12.8 % (for FPDPSAH) and 13.1 % (for WMDPSAH).

The variations of pressure drop in each SAH with mass flow rate are given in Fig. 16. When mass flow rate increases, flow velocity increases and consequently pressure drop increases in all conditions (Fig. 16). The maximum pressure drops were 34.6 N/m^2 in WMDPSAH, 28.2 N/m^2 in FPDPSAH, 26.4 N/m^2 in RPDPSAH and 6.8 N/m^2 in SPFPSAH for m = 0.04 kg/s. It is obvious that the pressure drop through the WFDPSAH is considerably higher than FPDPSAH, RPDPSAH and SPFPSAH due to the increased friction while employing wire mesh and 180° close return bend. Elkhawajah et al. [37] studied the performance of dual-pass SAH with wire mesh and transverse fins in the second channel and opined that pressure drop increases with mass flow rate and is in agreement with this study. The root mean square percent deviations (Eq. 59) between analytical and experimental results of pressure drop are 8.1 % (for SPFPSAH),

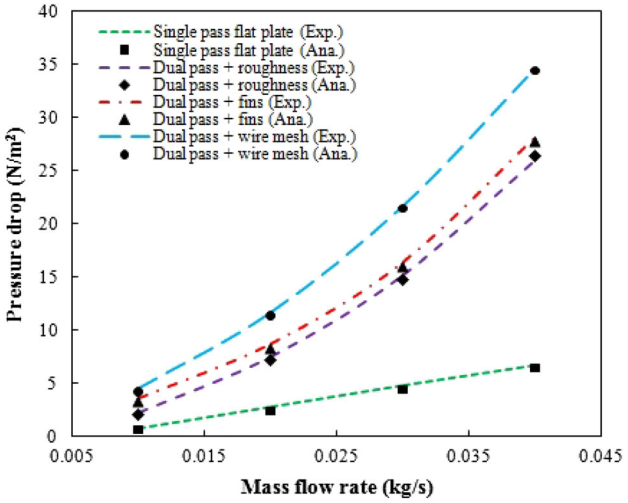

Fig. 16 Variation of pressure drop with mass flow rate

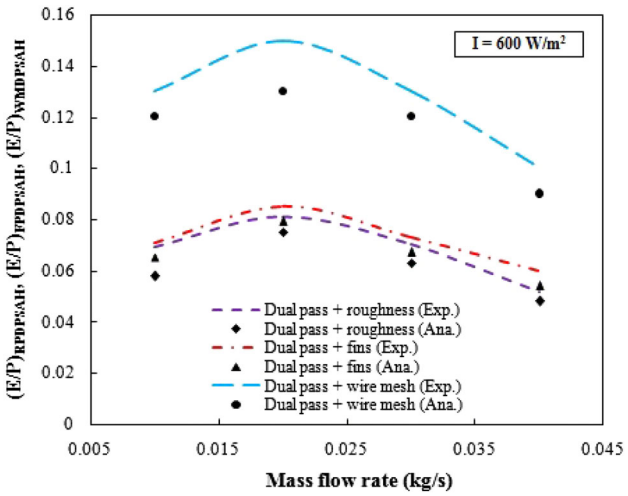

Fig. 17 Variation of E/P ratio with mass flow rate

4.7 % (for RPDPSAH), 4.9 % (for FPDPSAH) and 2.9 % (for WMDPSAH).

Figure 17 schematically illustrates the economic analysis of RPDPSAH, FPDPSAH and WMDPSAH by considering $(E/P)_{\text{RPDPSAH}}$, $(E/P)_{\text{FPDPSAH}}$ and $(E/P)_{\text{WMDPSAH}}$ with respect to mass flow rate of air. The value of $(E/P)_{\text{RPDPSAH}}$, $(E/P)_{\text{FPDPSAH}}$ and $(E/P)_{\text{WMDPSAH}}$ increases up to $m = 0.02$ kg/s and then decreases with increasing mass flow rate owing to larger power consumption increment. An economic mass flow rate of 0.02 kg/s is obtained in this study. The WMDPSAH is more economical than RPDPSAH and FPDPSAH due to the higher ratio of useful energy gain enhancement to power consumption increment at varied mass flow rate of air. The root mean square percent deviations (Eq. 59) between analytical and experimental results of E/P are 10.29 % (for RPDPSAH), 10.29 % (for FPDPSAH) and 10.07 % (for WMDPSAH).

9 Conclusion

This paper presents the analytical and experimental results of four different models of SAHs. The temperature rise of air decreases, whereas the energy efficiency increases with increasing mass flow rate of air. For WMDPSAH, a maximum efficiency of 76.46 % is obtained at $m = 0.04$ kg/s. The highest temperature rise of air obtained from this study is 25.2 °C for WMDPSAH at $m = 0.01$ kg/s. The introduction of v-corrugated wire mesh layer in the second pass of dual-pass mode creates turbulence intensity, enlarges the heat transfer area, increases the path length and reduces the top heat losses from the covers, thereby enhancing energy efficiency and temperature rise of air. The exergy output decreases and pressure drop increases with mass flow rate of air. The WMDPSAH exhibits better exergy output and higher pressure drop than other conditions. In addition, the temperature rise of air and exergy output increases with solar intensity (500–600 W/m^2), whereas energy efficiency is almost constant for all experimental conditions. The WMDPSAH is economically feasible compared with RPDPSAH and FPDPSAH. The analytical and experimental results are in fairly good agreement.

References

1. Azarpour, A.; Suhaimi, S.; Zahedi, G.; Bahadori, A.: A review on the drawbacks of renewable energy as a promising energy source of the future. Arab. J. Sci. Eng. **38**(2), 317–328 (2013)
2. Mohamad, A.A.; Alansary, H.; Orfi, J.: Natural convection between a vertical wall exposed to solar energy and a shaded wall. Arab. J. Sci. Eng. **39**, 9127–9136 (2014)
3. Das, K.; Durai, P.R.; Kundu, P.K.: Solar radiation effects on Cu–water nanofluid flow over a stretching sheet with surface slip and temperature jump. Arab. J. Sci. Eng. **39**, 9015–9023 (2014)
4. Prasad, S.B.; Saini, J.S.; Singh Krishna, M.: Investigation of heat transfer and friction characteristics of packed bed solar air heater using wire mesh as packed materials. Sol. Energy **83**, 773–783 (2009)
5. Alta, D.; Bilgili, E.; Ertekin, C.; Yaldiz, O.: Experimental investigation of three different solar air heater energy and exergy analyses. Appl. Energy **87**, 2953–2973 (2010)
6. Ozgen, F.; Esan, M.; Esan, H.: Experimental investigation of thermal performance of a double flow solar air heater having aluminium cans. Renew. Energy **34**, 2391–2398 (2009)
7. Ramani, B.M.; Gupta, A.; Kumar, R.: Performance of a double pass solar air collector. Sol. Energy **84**, 1929–1937 (2010)
8. Aldabbagh, L.B.Y.; Egelioglu, F.; Ilkan, M.: Single and double pass solar air heaters with wire mesh as packing bed. Energy **35**, 3783–3787 (2010)
9. Yeh, H.M.; Lin, T.T.: Efficiency improvements of flat plate solar air heaters. Energy **21**(7), 435–443 (1996)
10. Lin, W.; Gao, W.; Liu, T.: A parametric study on the thermal performance of cross-corrugated solar air collectors. App. Therm. Eng. **26**, 1043–1053 (2006)
11. Akpinar, E.K.; Koçyiğit, F.: Experimental investigation of thermal performance of solar air heater having different obstacle

on absorber plates. Int. Commun. Heat Mass Trans. **37**, 416–421 (2010)
12. Benli, H.: Experimentally derived efficiency and exergy analysis of a new solar air heater having different surface shapes. Renew. Energy **50**, 58–67 (2013)
13. Esan, H.: Experimental energy and exergy analysis of a double-flow solar air heater having different obstacles on absorber plates. Build. Environ. **43**, 1046–1054 (2008)
14. Yeh, H.M.; Ho, C.D.; Hou, J.Z.: Collector efficiency of double flow solar air heaters with fins attached. Energy **27**, 715–727 (2002)
15. Naphon, P.; Kongtragool, B.: Theoretical study on heat transfer characteristics and performance of the flat plate solar air heaters. Int. Commun. Heat Mass Trans. **30**, 1125–1136 (2003)
16. Sahu, M.M.; Bhagoria, J.L.: Augmentation of heat transfer coefficient by using 90° broken transverse ribs on absorber plate of solar air heater. Renew. Energy **30**, 2057–2073 (2005)
17. Karim, M.A.; Hawlader, M.N.A.: Performance investigation of flat plate, v-corrugated and finned air collectors. Energy **31**, 452–470 (2006)
18. Omojaro, A.P.; Aldabbagh, L.B.Y.: Experimental performance of single and double pass solar air heater with fins and steel wire mesh as absorber. Appl. Energy **87**, 3759–3765 (2010)
19. Rosen, M.A.: Using exergy to assess regional and national energy utilization: a comparative review. Arab. J. Sci. Eng. **38**, 251–261 (2013)
20. Yang, B.; Chen, L.; Ge, Y.; Sun, F.: Exergy performance optimization of an irreversible closed intercooled regenerative Brayton cogeneration plant. Arab. J. Sci. Eng. **39**, 6385–6397 (2014)
21. Karsli, S.: Performance analysis of new design solar air collectors for drying applications. Renew. Energy **32**, 1645–1660 (2007)
22. Gupta, M.K.; Kaushik, S.C.: Exergetic performance evaluation and parametric studies of solar air heater. Energy **33**, 1691–1702 (2008)
23. Yeh, H.M.: Upward-type flat-plate solar air heaters attached with fins and operated by an internal recycling for improved performance. J. Taiwan Inst. Chem. Eng. **43**, 235–240 (2012)
24. Ho, C.D.; Lin, C.S.; Chuang, Y.C.; Chao, C.C.: Performance improvement of wire mesh packed double-pass solar air heaters with external recycle. Renew. Energy **57**, 479–489 (2013)
25. Naphon, P.: On the performance and entropy generation of the double-pass solar air heater with longitudinal fins. Renew. Energy **30**, 1345–1357 (2005)
26. Verma, S.K.; Prasad, B.N.: Investigation for the optimal thermohydraulic performance of artificially roughened solar air heaters. Renew. Energy **20**, 19–36 (2000)
27. Varshney, L.; Saini, J.S.: Heat transfer and friction factor correlations for rectangular solar air heater duct packed with wire mesh screen matrices. Sol. Energy **62**(4), 255–262 (1998)
28. El-Sebaii, A.A.; Aboul-Enein, S.; Ramadan, M.R.I.; Shalaby, S.M. Moharram B.M.: Thermal performance investigation of double pass-finned plate solar air heater. Appl. Energy **88**, 1727–1739 (2011)
29. Dhiman, P.; Thakur, N.S.; Chauhan, S.R.: Thermal and thermohydraulic performance of counter and parallel flow packed bed solar air heaters. Renew. Energy **46**, 259–268 (2012)
30. Mittal, M.K.; Varshney, L.: Optimal thermohydraulic performance of a wire mesh packed solar air heater. Sol. Energy **80**, 1112–1120 (2006)
31. Velmurugan, P.; Kalaivanan, R.: Energy and exergy analysis of multi-pass flat plate solar air heater—an analytical approach. Int. J. Green Energy (2014). doi:10.1080/15435075.2014.888662
32. Al-Mutairi, E.M.: Retrofit and exergy analysis of fluid catalytic cracking unit using heat recovery approach temperature as decision criterion. Arab. J. Sci. Eng. **39**, 3403–3414 (2014)
33. Sun, W.; Ji, J.; He, W.: Influence of channel depth on the performance of solar air heaters. Energy **35**, 4201–4207 (2010)
34. Solanki, S.C.; Dubey, S.; Tiwari, A.: Indoor simulation and testing of photovoltaic thermal (PV/T) air collectors. Appl. Energy **86**, 2421–2428 (2009)
35. Ho, C.D.; Chang, H.; Wang, R.C.; Lin, C.S.: Performance improvement of a double-pass solar air heater with fins and baffles under recycle operation. Appl. Energy **100**, 155–163 (2012)
36. Ramadan, M.R.I.; EL-Sebaii, A.A.; Aboul-Enein, S.; El-Bialy, E.: Thermal performance of a packed bed double-pass solar air heater. Energy **32**, 1524–1535 (2007)
37. El-khawajah, M.F.; Aldabbagh, L.B.Y.; Egelioglu, F.: The effect of using transverse fins on a double pass flow solar air heater using wire mesh as an absorber. Sol. Energy **85**, 1479–1487 (2011)